

Highly sensitive breath sensor based on sonochemically synthesized cobalt-doped zinc oxide spherical beads

Chang Hee Cho^a, Yong-Sahm Choe^b, Soosang Chae^{c,*}, Tae Il Lee^{a,*}

^a Department of Materials Science and Engineering, Gachon University, Seong-nam, Gyeonggi 13120, Korea

^b iSenLab Inc. Dunchondae-ro 545, Jungwong-gu, Seong-nam, Gyeonggi, Korea

^c IPF - Leibniz-Institut für Polymerforschung Dresden e.V., Institute of Physical Chemistry and Polymer Physics, 01069 Dresden, Germany

ARTICLE INFO

Keywords:

Sonochemical synthesis
Metal oxide
Co-doped ZnO
Acetone sensor
Exhalation diagnostic

ABSTRACT

In this study, we introduce cobalt (Co)-doped zinc oxide (ZnO) spherical beads (SBs), synthesized using a sonochemical process, and their utilization for an acetone sensor that can be applied to an exhalation diagnostic device. The sonochemically synthesized Co-doped ZnO SBs were polycrystalline phases with sizes of several hundred nanometers formed by the aggregation of ZnO nanocrystals. As the Co doping concentration increased, the amount of substitutionally doped Co²⁺ in the ZnO nanocrystals increased, and we observed that the fraction of Co³⁺ in the Co-doped ZnO SBs increased while the fraction of oxygen vacancies decreased. At an optimal Co-doping concentration of 2 wt%, the sensor operating temperature decreased from 300 to 250 °C, response to 1 ppm acetone improved from 3.3 to 7.9, and minimum acetone detection concentration was measured at 43 ppb (response, 1.75). These enhancements are attributed to the catalytic role of Co³⁺ in acetone oxidation. Finally, a sensor fabricated using 2 wt% Co-doped ZnO SBs was installed in a commercially available exhalation diagnostic device to successfully measure the concentration of acetone in 1 ml of exhaled air from a healthy adult, returning a value of 0.44 ppm.

1. Introduction

Obesity is a complex disease accompanied by an excessive amount of body fat and has been recognized to increase the risk of heart disease, diabetes, high blood pressure, and various cancers [1–3]. Many people today, regardless of age or sex, are suffering from obesity owing to excessive carbohydrate intake. Combined with exercise, the ketogenic diet, wherein fats and not carbohydrates are broken down and used as the main energy source to lose weight, can effectively resolve obesity [4–6]. The ketogenic-diet-related market is currently worth \$10 billion and is expected to reach \$15 billion by 2027 [7].

Conventionally, monitoring of VOCs is of important in many application field such as fire detection, lab safety, indoor air quality and environmental monitoring [8,9]. Various types of volatile organic compounds (VOCs) are emitted by exhalation from the human body. Interestingly, these VOCs can be used as biomarkers to identify health conditions [10,11]. A typical example is the measurement of blood ethanol concentration through the concentration of ethanol in exhaled air [12]. In the case of a ketogenic diet, the breakdown of fat increases the concentration of acetoacetate (AcAc) in the blood, which is then

metabolized into β-hydroxybutyrate (BHB) and acetone [13]. A strong correlation has been reported between the concentration of acetone in exhaled breath and amount of BHB present in blood [14]. Based on this correlation, the degree of lipolysis can be monitored by measuring the concentration of acetone in the exhaled breath, which is approximately 2–40 ppm in the case of BHB [15].

Monitoring lipolysis is important for the treatment of obesity. To measure the degree of body fat breakdown according to the amount of acetone in exhalation, various methods, such as mass spectrometry, photoionization, gas chromatography, light-addressable potentiometric sensors, quantum cascade lasers, and semiconductor metal oxide sensors, have been studied [16]. Among them, semiconductor metal oxide sensors are a suitable technology for portable acetone exhalation analyzers that monitor ketogenic diets because they are inexpensive, have excellent sensitivity, and enable miniaturization of the measuring equipment.

It is known that in healthy adults, an exhaled acetone concentration of 0.3 to 1.2 ppm is typically observed when the person is not on a ketogenic diet [17]. Considering the volume of normal exhalation, it is desirable to detect acetone even when the exhalation volume is as small

* Corresponding authors.

E-mail addresses: chae@ipfdd.de (S. Chae), t2.lee77@gachon.ac.kr (T. Il Lee).

<https://doi.org/10.1016/j.ultsonch.2022.105956>

Received 28 December 2021; Received in revised form 22 January 2022; Accepted 14 February 2022

Available online 16 February 2022

1350-4177/© 2022 The Author(s).

Published by Elsevier B.V. This is an open access article under the CC BY-NC-ND license

(<http://creativecommons.org/licenses/by-nc-nd/4.0/>).

as possible. Therefore, the sensor requires sufficient sensitivity to measure the ppb level of acetone gas in 1 ml of exhalation. In addition, it is necessary to lower the operating temperature of the sensor to achieve low power consumption for instrument miniaturization.

To meet these requirements, we introduce sonochemically synthesized cobalt (Co)-doped zinc oxide (ZnO) spherical beads (SBs) in this study. The sonochemically synthesized ZnO showed a spherical shape of several hundred nanometers formed by the accumulation of very small nanoparticles of 14–15 nm. Interconnection of the spherical ZnO beads allowed for highly sensitive gas sensors due to the very narrow connection point between beads, leading to a large change in the resistance during gas detection.

Furthermore, to lower the sensor working temperature and further increase the sensitivity, Co was doped as a catalyst. The Co-doped ZnO SBs exhibited a high response to acetone, along with lowered the working temperature of the sensor. The fabricated sensor was mounted on a commercial expiratory diagnostic equipment to monitor 1 ml of exhaled breath from a healthy adult, which successfully measured a concentration of acetone of 0.4 ppm.

2. Material and methods

2.1. Material preparation

Co-doped ZnO SBs were sonochemically synthesized via tip sonication. First, 0.25 g of Mw 20,000 polyethylene glycol (PEG, Samchun Chemicals) was dissolved in 25 ml of deionized (DI) water through stirring at 60 °C overnight. Subsequently, 0.1125 g of zinc nitrate hexahydrate (98%, Alfa Aesar) was dissolved in the solution, and cobalt acetate tetrahydrate (98%, Daejung) was added to the solution at the concentrations of 1 wt% (2.5724 mg), 2 wt% (5.1448 mg), and 3 wt% (7.7172 mg) Co to Zn. Thereafter, 0.5 ml of triethanolamine (TEA, 99%, Daejung) was added. The solution was sonicated using a titanium tip (6 mm in diameter, 20 kHz, Q700 Qsonica) at 10 W for 40 min. Approximately 10 min later, the transparent solution became cloudy, and a milky solution was obtained. After synthesis, the solution was centrifuged (10,000 rpm, 15 min), and the supernatant was replaced with ethanol. This process was repeated three times for purification, and the obtained Co-doped ZnO SBs were stored in pure ethanol for future use.

2.2. Material characteristics

For the optical analysis, a UV–VIS spectrophotometer (JASCO V-770) at the Core Facility for Bionano Materials at Gachon University was used to measure the reflectance of the Co-doped ZnO SB films. For the X-ray analysis, high-resolution X-ray diffraction (HR-XRD, Rigaku Corporation SmartLab) was used for crystallographic assessment of the particles. The chemical composition of the Co-doped ZnO SBs were determined using X-ray photoelectron spectroscopy (XPS, Thermo Scientific Inc., UK, K-alpha) with monochromatic Al-K α (1486.6 eV). For the morphology analysis, a scanning electron microscope (SEM, HITACHI S-4300) was used to observe the shape of the Co-doped ZnO SBs and distribution of their sizes. High-resolution transmission electron microscopy (HRTEM, JEOL JEM F-200) with energy dispersive X-ray spectrometry (EDS) was used to observe the microstructure and chemical composition of a Co (2 wt%)-doped ZnO SB.

2.3. Sensor fabrication and performance

For the sensor fabrication, an alumina substrate, where Pt electrodes were located on the top and a Pt heating line was on the bottom, was used. Pt wires were soldered at the end of each electrode to measure the sensor resistance, and at both ends of the heating line, to heat the substrate. A well-dispersed Co-doped ZnO SB solution in DI water was drop-casted on the substrate and evaporated the DI water slowly. Then, the sensor was annealed at 500 °C for 1 h in ambient air (a photo of the

fabricated sensor device as shown in Fig. S7 of Supplementary Information).

To measure the performance of the Co-doped ZnO SB sensor in acetone gas, the sensor was mounted on a stage with cylindrical four-terminal electrodes and installed in a Teflon chamber. To provide electric current as a heat source, two terminals of the heating line were connected to a direct current (DC) power supply (MKPOWER MK3005P). To measure the time-dependent resistance change of the sensor, the other two terminals of the sensor electrodes were connected to a parameter analyzer (KEITHLEY 4200A-SCS). A mixture of dry air (99.99%) and N₂ (99.99%) was used as the reference gas, and a mixture of dry air (99.99%) and N₂ balanced with 2 ppm (or 100 ppm) acetone was used as the target gas. The total gas flow was 100 standard cubic centimeter per minute (sccm), and the acetone gas concentration was set by controlling the flow ratio of dry air and N₂-balanced acetone with a mass flow controller. For example, 1 ppm of acetone gas was prepared by flowing 50 sccm of dry air and 50 sccm of N₂ balanced with 2 ppm acetone. The response was defined as R_a/R_g , where R_a is the resistance measured by the reference gas flow and R_g is the resistance measured by the target gas flow. The response and recovery times were defined as the time required for a 90% change in the sensor resistance after the target gas was turned on or off.

2.4. Demonstration

The sensor was installed and tested in a commercialized exhalation diagnosis device made by iSenLab Inc. to demonstrate the feasibility of a Co-doped ZnO SB sensor for monitoring ketogenic diets in humans. Only 1 ml of human breath was captured via this device. Using the gas separation system equipped in the device, the acetone gas present from the breath reacted with the Co-doped ZnO SB sensor, and the calibrated response of the sensor was measured. Finally, the concentration of acetone in the breath was estimated from the measured value of the response compared to that of 2 ppm acetone gas.

3. Results and discussion

3.1. Overall fabrication process

The overall fabrication process of the Co-doped ZnO SB sensor is displayed in Fig. 1. Co-doped ZnO SBs were synthesized using a sonochemical method in an aqueous solutions of zinc nitrate hexahydrate, cobalt acetate tetrahydrate, PEG, and TEA. Co-doped ZnO SBs with uniform spherical shapes for each mass fraction of Co were synthesized by ultrasonication for 40 min. After synthesis, the three-time purified Co-doped ZnO SBs, were drop-cast onto the sensor substrate and annealed for 1 h. A structure of uniformly stacked SBs is advantageous as a gas sensor in terms of geometry and electrical resistance. A structure formed by making point contact with numerous SBs has excellent permeability to external gases and provides a large specific surface area. In addition, in terms of electrical resistance, the contact point between SBs results in high contact resistance, thus, it can effectively reflect changes in the electrical conductivity of particles according to the adsorption of gas species as large changes in the sensor resistance.

3.2. Material analysis

3.2.1. Optical analysis

After annealing, the color of the Co-doped ZnO SBs became blue-green, and the color shade became deeper with increasing Co-doping concentrations, as depicted in Fig. S1 of the Supplementary data. To determine the reason for this apparent color change, an optical analysis of the Co-doped ZnO SB films on a glass substrate was performed, whose results are presented in Fig. 2. Fig. 2(a) shows the reflectance of the films with different Co-doping concentrations. As the Co-doping concentration increased, the absorption intensities (inverse of reflectance) of the

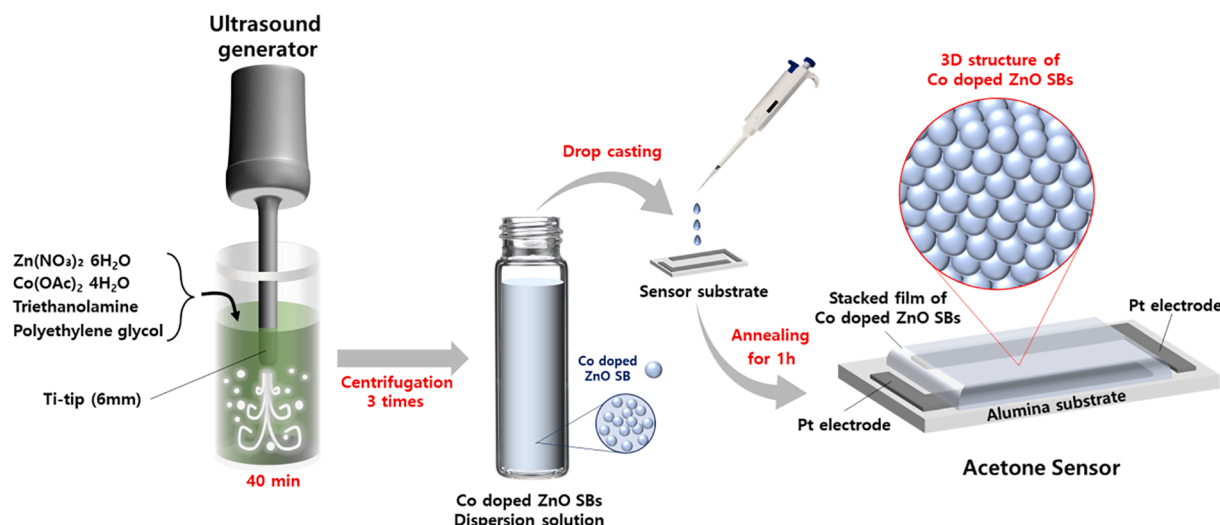


Fig. 1. Schematic illustrating the overall fabrication process of the Co-doped ZnO SB acetone sensor.

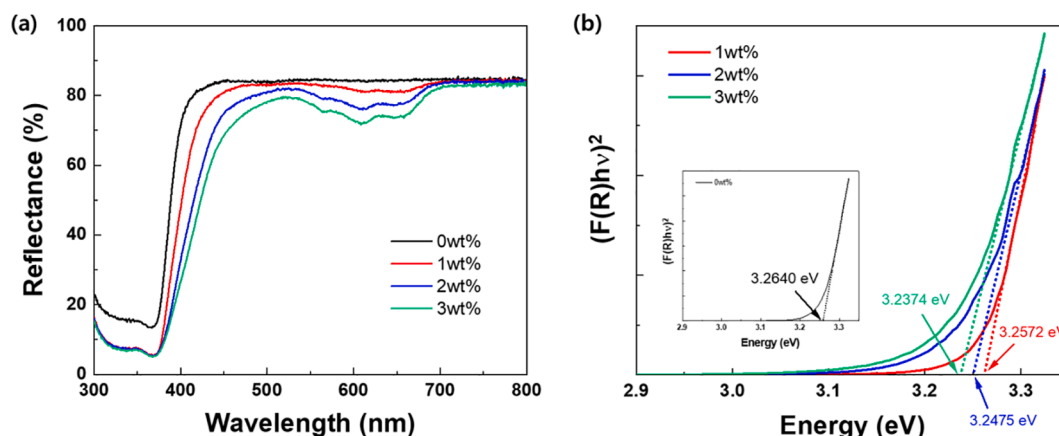


Fig. 2. (a) Reflectance and (b) optical band gap of Co-doped ZnO SB films with different Co-doping concentrations.

peaks measured at 570, 610, and 655 nm also increased. These peaks are attributed to the d-d internal electronic transitions of Co^{2+} ions that are tetrahedrally coordinated in a crystal [18]. This result indicates that Co-doping occurs in a substitutional form, wherein Co^{2+} replaces the Zn^{2+} sites in the ZnO crystal. As the doping concentration increased, the number of substitution sites increased; hence, the corresponding peaks increased.

Considering that the rate of change of reflectance with respect to the wavelength in the vicinity of 400 nm gradually decreased, the change in the optical bandgap with respect to the Co-doping concentration was quantitatively analyzed. To calculate the optical band gap of each film from reflectance measurements, the Kubelka–Munk function was used [19,20]. The Kubelka–Munk function (F_{KM}) was calculated from the reflectance spectra (R_{diff}). The absorption coefficient was calculated (α).

$$F_{\text{KM}} = \frac{(1 - R_{\text{diff}})^2}{2R_{\text{diff}}} \propto \alpha$$

The calculation of optical band gap is based on linear fits of $(\alpha \cdot h\nu)^n$ vs. $h\nu$ plots, where $h\nu$ is photo energy. The conversion graph and optical band gap of each Co-doped ZnO SB are shown in Fig. 2(b). The red, blue, and green lines represent the Kubelka–Munk curves of 1, 2, and 3 wt% Co-doped ZnO SBs, respectively. The inset demonstrates the curve for undoped (0 wt%) ZnO SBs. The optical bandgaps of 0, 1, 2, and 3 wt% Co-doped ZnO SBs were 3.2640, 3.2572, 3.2475, and 3.2374 eV, respectively. This indicated a decreasing trend as the concentration

increased. The decrease in the band gap is caused by the sp-d exchange interactions between the electrons within the energy band of ZnO and those in the d orbital of Co^{2+} [21].

The decrease in reflectance for these peaks creates a lack of the red wavelength to the naked eye under white-light illumination. In addition, the decrease in the optical band gap results in a decrease in the reflectance of the relative blue wavelength. These two phenomena are attributable for the color change of Co-doped ZnO SBs from the apparent color to green, as the doping concentration increases.

3.2.2. Electron microscope analysis

Fig. 3 shows top view SEM images of Co-doped ZnO SB drop-cast films with various Co-doping concentrations. The synthesized ZnO exhibited a uniform spherical shape under all doping conditions. As the Co-doping concentration increased, the diameter demonstrated a tendency to gradually decrease. An accurate statistical analysis of the diameter change was performed, whose results are presented in Fig. S2 of the Supplementary data. The diameter of the sphere decreased from 525 to 475 nm with an increasing doping concentration, and for each doping concentration level, the standard deviation of the diameter size was analyzed to be approximately 5 to 8%.

Fig. 4(a) and (b) present TEM images of the 2 wt% Co-doped ZnO SB. From the TEM images, we confirmed that the ZnO SBs had a microstructure in which many small nanocrystals were gathered in a spherical shape with a diameter of several hundred nanometers (Fig. 4a). From the

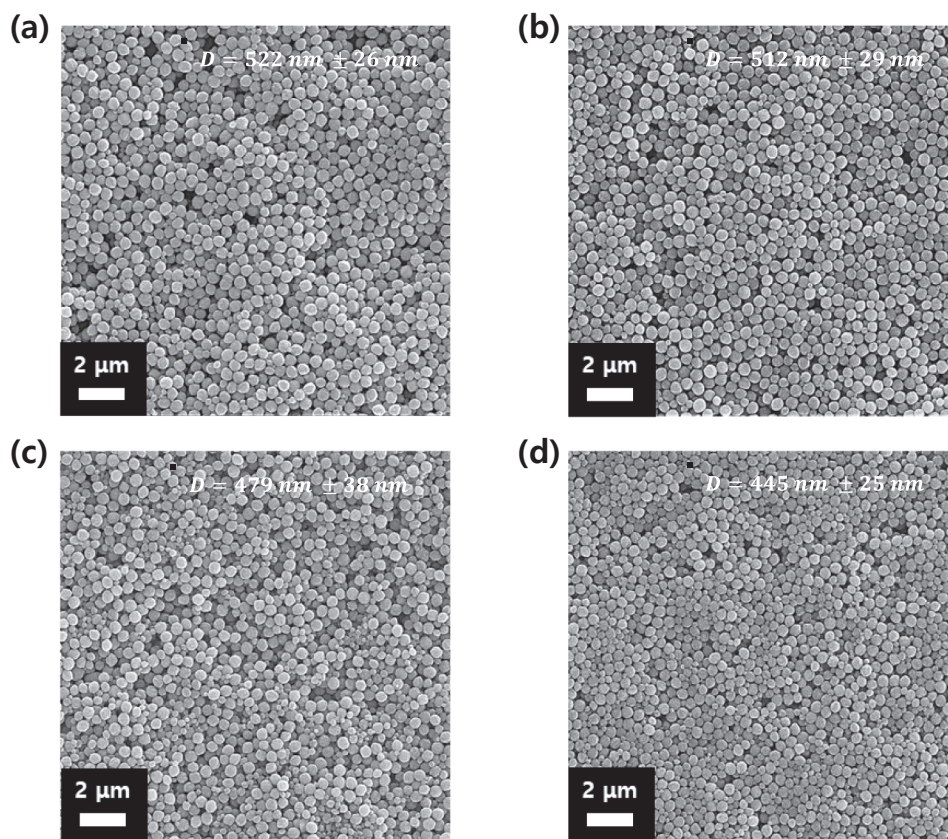


Fig. 3. Top view SEM images of the Co-doped ZnO SBs with various doping concentrations: (a) 0, (b) 1, (c) 2, and (d) 3 wt%.

HRTEM image, we found that the nanocrystals represent the (0002) interplanar distance of a typical ZnO wurtzite structure of 0.272 nm (Fig. 4b). However, no crystal phase of the oxide related to Co was observed. EDS analysis was performed to detect the Co component distributed in the Co-doped ZnO SB, whose results are reported in Fig. 4(c). The analysis results show that Co was evenly distributed throughout a ZnO SB.

3.2.3. X-ray analysis

The XRD patterns of the Co-doped ZnO SBs were measured to observe the crystallographic changes owing to Co-doping. Fig. 5 demonstrates the HR-XRD patterns of the Co-doped ZnO SBs with different doping concentrations. All diffraction peaks agree well with the ZnO in the JCPDS database (card no. 00–036–1451), where other peaks are not shown. The average crystal sizes for 0, 1, 2, and 3 wt% Co-doped ZnO SBs were calculated using the Scherrer equation, whose results are presented in Fig. S3 of the Supplementary data. Regardless of the Co-doping concentration, the average diameter of the grains of all synthesized Co-doped ZnO SB was measured to be approximately 14 nm. The Co-doping in the ZnO lattice was performed in such a manner that Zn²⁺ substituted Co²⁺. However, because the ionic radii of Zn²⁺ and Co²⁺ are 0.74 and 0.75 Å, respectively, the difference in the radius between the two ions is almost negligible. Subsequently, the crystallographic change of ZnO before and after Co-doping was rarely observed.

To investigate the compositional changes of the Co-doped ZnO SBs with respect to the doping concentration, XPS analysis was performed. Fig. 6 presents the XPS data of the Co-doped ZnO SBs with various doping concentrations. Fig. 6(a) depicts Zn 2p peaks. For all doping concentrations, the Zn 2p_{3/2} and Zn 2p_{1/2} peaks were equally located at the binding energy levels of 1021.57 and 1044.67 eV, respectively. Co 2p peaks are reported in Fig. 6(b) and (c), where the Co 2p_{3/2} and Co 2p_{1/2} peaks appear at 781.17 and 796.67 eV, respectively, except for undoped ZnO SB (0 wt%). The intensities of peaks increase with

increasing doping concentrations. The results of the further analysis of the Co 2p peaks at each Co-doping concentration are shown in Fig. 6(c). The black ring symbol denotes the raw data, red line denotes the fitted data, and blue, green, and pink lines indicate the Co³⁺, Co²⁺, and satellite peaks, respectively. Interestingly, the signal of the Co³⁺ ratio becomes larger than that of Co²⁺ with increasing doping concentrations. O 1 s peaks are reported in Fig. 6(d), and the blue, green, and pink lines denote the metal-bonded oxygen in the lattice, oxygen vacancy (O_v), and surface-absorbed oxygen (O_A), respectively. The deconvolution results of O 1 s peaks indicated that the fraction of O_v decreased with increasing Co-doping concentrations.

The peculiarity of the compositional change with increasing Co-doping concentration was that the Co³⁺ fraction increased while the O_v fraction decreased in the Co-doped ZnO SBs. The quantitative analysis results related to compositional changes are summarized in Fig. 7. Although no diffraction peak corresponding to Co₃O₄ was observed in the XRD results presented in Fig. 5, the increase in the Co³⁺ fraction in the XPS spectra indicated that Co₃O₄ existed inside a Co-doped ZnO SB. Because the amount of Co₃O₄ is insignificant, it seems that Co₃O₄ could not grow to a sufficiently large grain to be observed in HRTEM or XRD. Therefore, we thought that the Co²⁺ mainly employed in the Co-doped ZnO SB synthesis transformed into a substitutional dopant in the ZnO lattice, considering the results of the reflectance and optical bandgap analysis. Furthermore, the Co²⁺ ions were converted into Co₃O₄, as observed from the XPS results. In other words, as the doping concentration increased, the fraction of Co³⁺ approached 60% and saturated, which is similar to the fraction value of Co³⁺ in the Co₃O₄ spinel crystal structure. The decrease in O_v fraction can be understood through analyzing the microstructure of the ZnO SBs. In the case of the undoped ZnO SB, the fraction of O_v was 50%. A material with a polycrystalline phase and an O_v fraction of 50% inevitably has a large area of grain boundaries. From the HRTEM analysis results, we confirmed that the undoped ZnO SB was formed by aggregating about 14 nm sized ZnO

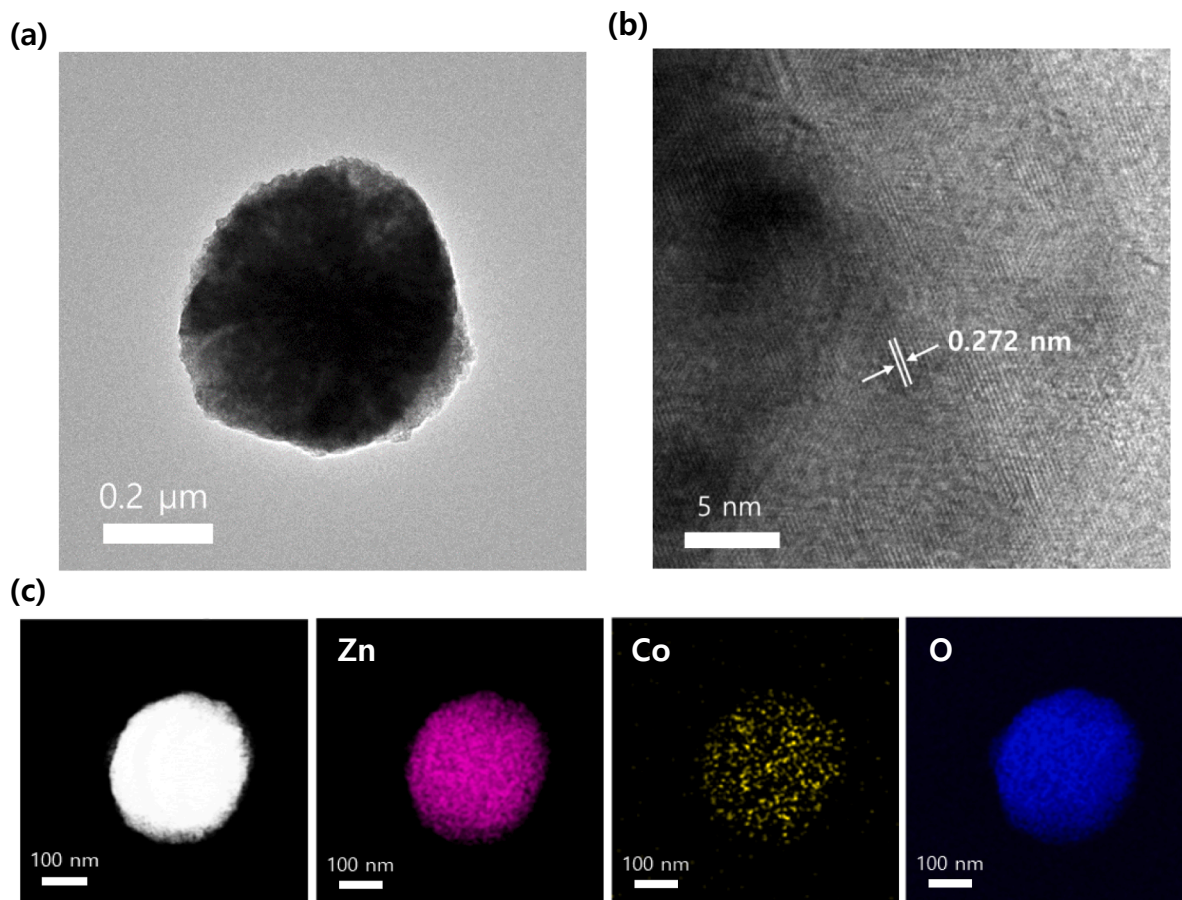


Fig. 4. (a) TEM, (b) HRTEM, and (c) EDS profiles of the 2 wt% Co-doped ZnO SB. From the left: electron image, Zn, Co, and O.

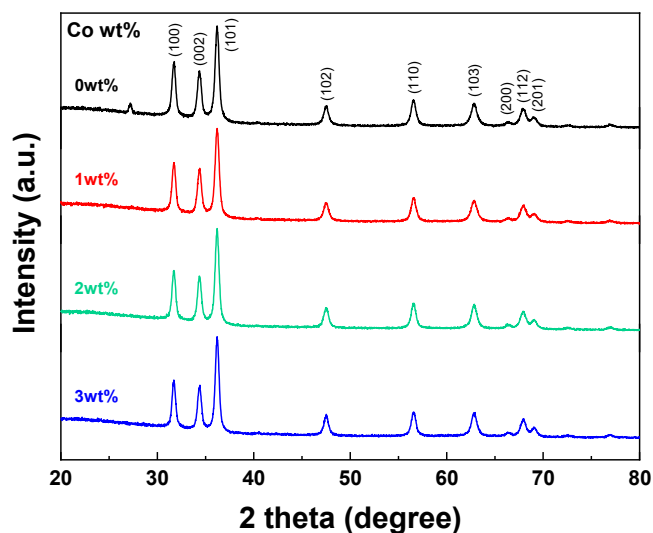


Fig. 5. HR-XRD patterns of Co-doped ZnO SBs with doping concentration.

nanocrystals, and there were numerous grain boundaries inside the SBs. The Co_3O_4 produced during the synthesis process could reside in the grain boundaries and lower the fraction of O_v in the Co-doped ZnO SBs. This hypothesis is supported by the result that the average diameter of the Co-doped ZnO SBs gradually decreased as the Co mass fraction increased.

(b)

3.3. Synthesis mechanism

When ultrasonic waves are irradiated to the solution during the synthesis, high temperatures and pressures are generated owing to acoustic cavitation. This large energy input by ultrasonic waves is sufficient to cause oxidation, reduction, dissolution, and decomposition reactions in the solution [22–25].

In the ultrasonic synthesis of metal oxides, there are two well-known mechanisms: sonochemical oxidation and hydrolysis [26]. In sonochemical oxidation, water is pyrolyzed by ultrasound to form hydrogen and hydroxyl radicals, which react with each other to form hydrogen and hydrogen peroxide. The hydrogen peroxide produced in this manner oxidizes the metal ions in the solution to form a metal oxide. In this case, Fe^{2+} and Co^{2+} typically follow the same mechanism. On the other hand, in sonochemical hydrolysis, metal ions are hydrolyzed to form hydroxide, followed by a dehydration reaction to form an oxide. In this case, Cu^{2+} and Zn^{2+} typically follow this mechanism.

In this study, the synthesis of ZnO was carried out using the following reaction equation using the sonochemical hydrolysis mechanism.



Cobalt doping is thought to substitute the defects in ZnO crystals during the synthesis process. In addition, when the concentration of Co^{2+} is high, the synthesis of Co_3O_4 , Co^{3+} was produced by the sonochemical oxidation mechanism, as follows:



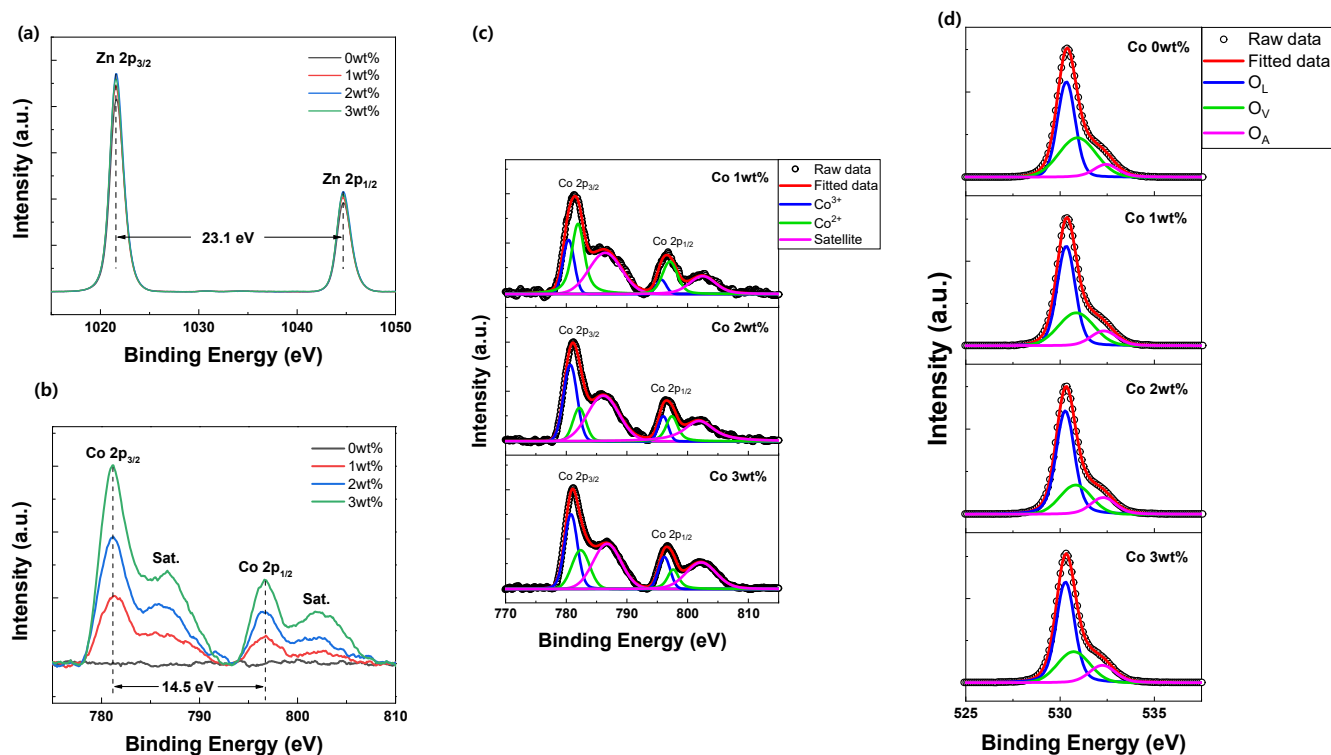


Fig. 6. XPS spectra of (a) Zn 2p and (b, c) Co 2p. (d) O1s from Co-doped ZnO SBs with various doping concentrations.

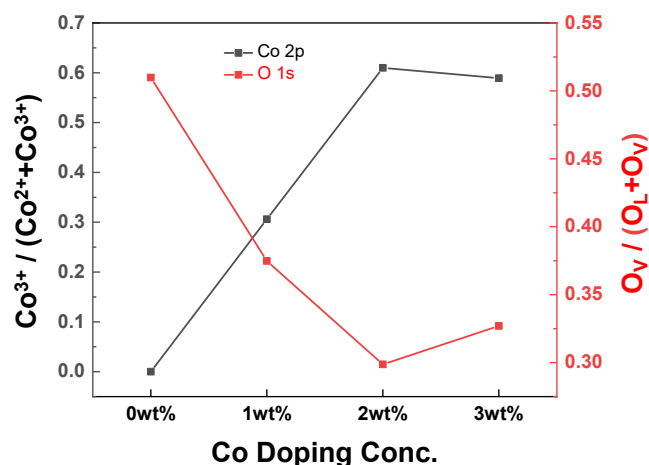


Fig. 7. Fractions of Co³⁺ and O_V with increasing Co-doping concentrations.

3.4. Acetone sensing performance

There was a compositional change in the Co-doped ZnO SBs with increasing Co-doping concentration. To investigate how the change in the composition affects the performance of the acetone sensor material, the optimal working temperature of the sensor for each Co-doping concentration was estimated. The optimum temperature is measured when the highest response to acetone is observed; in this study, the response to 1 ppm acetone is evaluated. Fig. 8 presents the optimal working temperature for sensors made of Co-doped ZnO SBs with various Co-doping concentrations. The optimal temperature for the undoped ZnO SB (0 wt%) sensor was 300 °C, where the best response value was approximately 5. The best response of the 1 wt% Co-doped ZnO SB sensor was observed at 300 °C, which was the same as that of the undoped ZnO SB. However, its response was larger than that of the

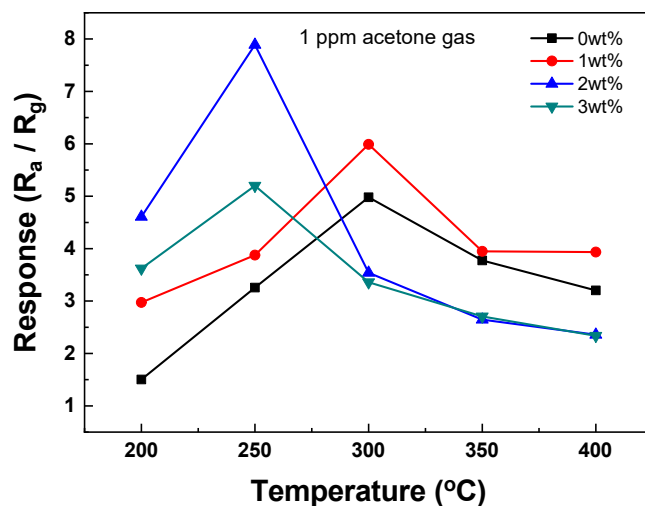


Fig. 8. Temperature-dependent response to the 1 ppm acetone gas of the Co-doped ZnO SB sensor at various Co-doping concentrations.

undoped ZnO SB sensor. The 2 and 3 wt% Co-doped ZnO SB sensors responded the best at 250 °C, with response values of 7.9 and 6.3, respectively. As a result, the sensor with the lowest operating temperature and the highest response was fabricated with 2 wt% Co-doped ZnO SB. The time-response curves of each Co-doped ZnO SB sensor are plotted in Fig. S4 of the Supplementary data, whose response and recovery times calculated from the time-response curve for 1 ppm acetone at 250 °C are reported in Table S1 of the Supplementary data. The response and recovery times of the sensor were not dependent on the Co-doping concentration. Presumably, the spherical shape of ZnO SB might have contributed to determining the response and recovery times, irrespective of the Co doping.

Fig. 9 depicts the performance of the 2 wt% Co-doped ZnO SB sensor

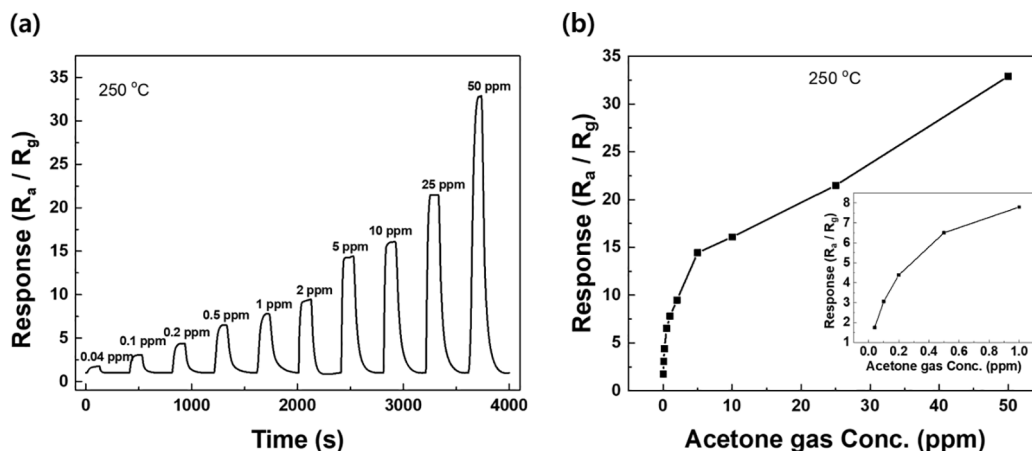


Fig. 9. (a) Time-response curve of the 2 wt% Co-doped ZnO SB sensor as a function of the acetone concentration at 250 °C. (b) Response of the 2 wt% Co-doped ZnO SB sensor to acetone below 1 ppm at 250 °C.

in detecting acetone gas at 250 °C. Fig. 9(a) presents the time-response curves. Fig. 9(b) shows a plot of the response as a function of the acetone gas concentration, where the inset shows the response characteristics of the 2 wt% Co-doped ZnO SB sensor for acetone gas below 1 ppm. The required detection range for acetone gas to monitor the effectiveness of the ketogenic diet is 0.5 to 40 ppm. Considering these margins, we measured the response to acetone gas in the range of 0.04–50 ppm. The 2 wt% Co-doped ZnO SB sensor yielded a response value of 33 at 50 ppm and 1.75 at 0.04 ppm. These results imply that our sensor, which shows a high response even at such low concentrations of acetone gas, has sufficient potential to monitor the effect of a ketogenic diet. In addition to the high response at low concentrations, long-term stability, which is a performance requirement of a sensor for monitoring the effect of a ketogenic diet, was evaluated under the condition of 1 ppm acetone gas at 250 °C for 30 days, whose results are presented in Fig. S5 of the Supplementary data. The response of the 2 wt% Co-doped ZnO SB sensor was stably maintained for 30 days.

In addition to response and long-term stability, selectivity is an important performance requirement for gas sensors. However, it is difficult to secure the selectivity of resistance-change-based semiconductor gas sensors. When any kind of gas is adsorbed by the sensor, only a difference the semiconductor sensor temperature is observed; however, in principle, a reaction slight takes place. Because the exhalation of the human body contains numerous gaseous species, including water, it is difficult to ensure selectivity in a commercial exhalation diagnostic instrument. In reality, to fundamentally rule out the problem of selectivity, it is essential to apply a gas separation system to the exhalation diagnostic device. Therefore, this study focused on developing a sensor with good long-term stability and high response for respiratory diagnosis.

3.5. Demonstration

It was demonstrated that the 2 wt% Co-doped ZnO SB sensor has a high response to 1 ppm or less acetone. To determine whether it is possible to detect acetone gas in human exhalation beyond the detection of pure acetone gas for laboratory use, we applied the sensor to a commercial expiratory diagnostic device to measure the concentration of acetone gas in 1 ml of exhaled air from a healthy adult. A commercial expiratory diagnostic device for the experiment was provided by iSen-Lab, Inc. Fig. S6 of the Supplementary data presents a camera image of the provided exhalation diagnostic device and conceptual diagram of the system configuration. When 1 ml of exhaled air is captured, all the gases present in the exhaled air arrive at the sensor chamber at different velocities with a time difference caused by the gas separation device. The time required for acetone gas to reach the sensor chamber can be

determined from the known time difference information. At this time, the gaseous acetone reacts with the sensor installed in the sensor chamber reacts and changes its resistance, and the result is measured as an electrical signal.

Before detecting acetone gas concentration present in a human body, the response to 2 ppm acetone gas was measured at 250 °C as a reference. Then, 1 ml of human exhalation was injected into the device, and the response was measured; the results are reported in Fig. 10. Fig. 10(a) shows the camera images of the exhalation diagnosis device with acetone sensing signals; the left image is the response to 2 ppm acetone gas, and image is the response to exhalation from a healthy adult. Fig. 10 (b) shows the time-response curves of our sensor for 2 ppm acetone and exhalation of a healthy adult. By comparing the response to 2 ppm acetone gas and exhalation of a healthy adult, we successfully estimated the concentration of acetone in the exhalation as 0.44 ppm, which is within the range of commonly known values for the concentration of acetone in the exhaled air of healthy adults. Therefore, this result indicates that our sensor is effective for measuring acetone concentrations human exhalation. Even though only 1 ml of exhalation was used, the Co-doped ZnO SB sensor successfully detected sub-ppm levels of acetone in the exhalation. Therefore, we believe that our sensor has great potential as a highly sensitive acetone detector for exhalation diagnosis.

3.6. Gas sensing mechanism

The acetone sensing mechanism of the Co-doped ZnO SB sensor and the catalytic effect of Co ions are summarized in Fig. 11. When the atmosphere in the sensor chamber changes from air to acetone, the resistances of all sensors decrease, indicating that both the ZnO SBs and Co-doped ZnO SBs are n-type semiconductors. An n-type semiconductor generally has free electrons in the conduction band as major carriers. In air, oxygen molecules are adsorbed on the surface of n-type semiconductors and are reduced by free electrons to form oxygen anions, resulting in the formation of an electron depletion layer near the surface. The sensor in air has a fixed resistance value in the saturated state of oxygen adsorption.

As shown in the HRTEM image presented in Fig. 4(b), the ZnO SB results from the aggregation of the ZnO nanocrystals. The electron transportation inside a ZnO SB is achieved by passing through the ZnO nanoparticles. The electron depletion layer acts as an energy barrier against electrons crossing the boundary between the ZnO nanoparticles, contributing to an increase in the resistivity of the ZnO SBs. As the number of electron depletion layers increased, the energy barrier between the ZnO nanoparticles increased. In addition, the stacked ZnO SBs form a three-dimensional network structure over the sensor terminal electrodes, and the contact resistance between the ZnO SBs is considered

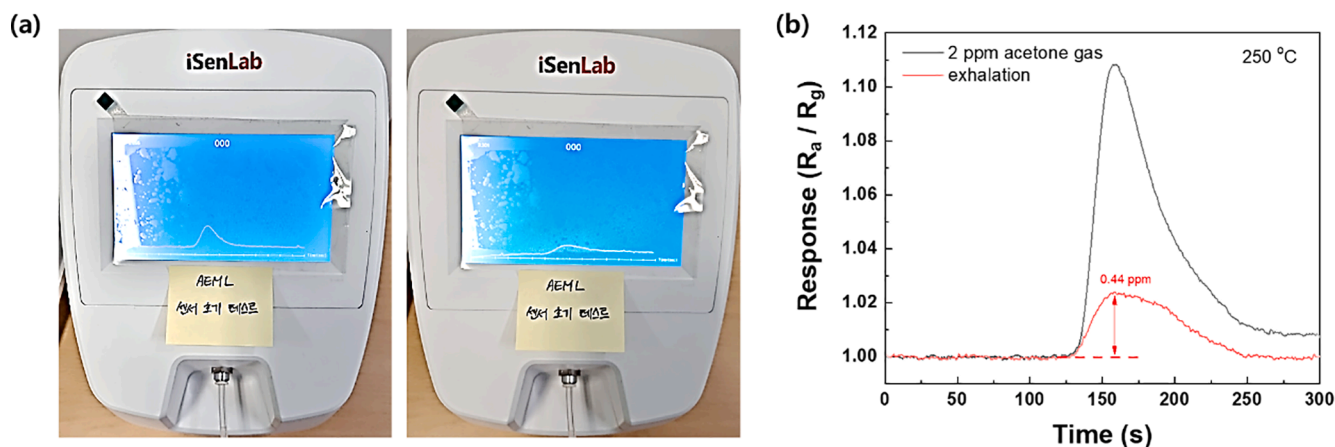


Fig. 10. (a) The camera images of signals on display window of the exhalation diagnosis device. Left is the result of response to 2 ppm acetone gas and right is the result of response to exhalation of a healthy adult. (b) The time-response curves measured by the exhalation diagnosis device for 2 ppm acetone gas and exhalation of a healthy adult.

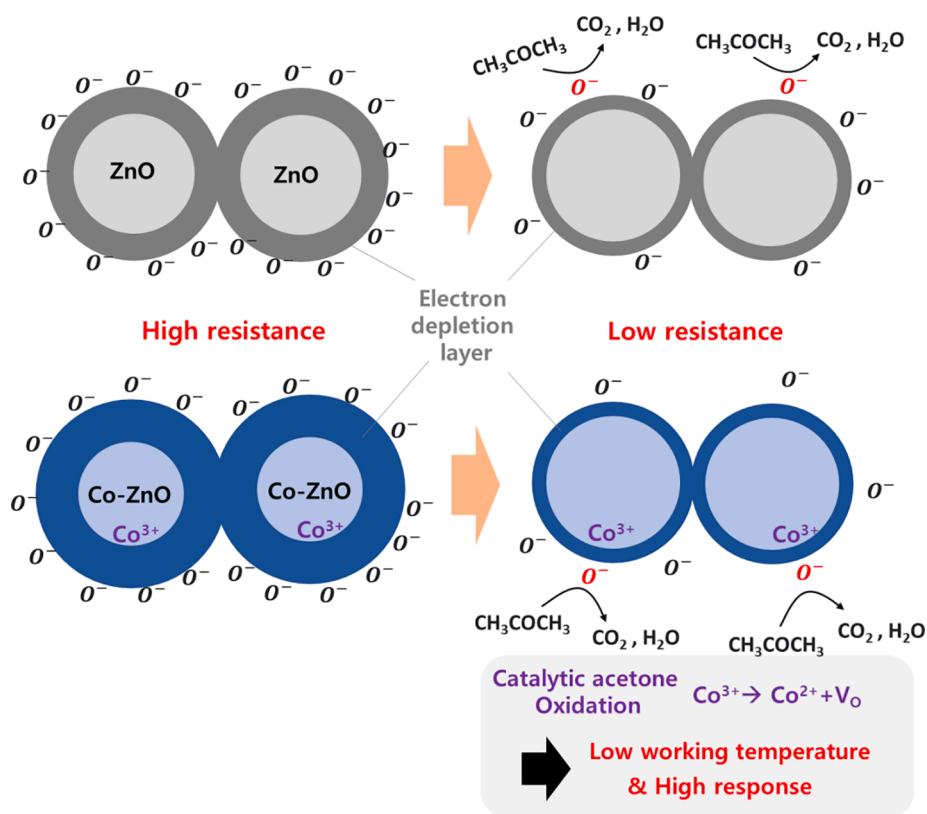


Fig. 11. Acetone sensing mechanism and catalytic oxidation of acetone.

another energy barrier for the transportation of electrons. This barrier also increased as the thickness of the electron depletion layer increased.

When acetone is injected into the chamber, it reacts with the oxygen adsorbed by the surface to decompose into water and carbon dioxide. This reaction, which removes the oxygen adsorbed by the surface, occurs simultaneously with the reduction reaction of oxygen. These two reactions reach a state of dynamic equilibrium. Consequently, in the presence of acetone, the amount of oxygen adsorbed by the surface decreases, and the electron depletion layer becomes thinner. The acetone concentration around the sensor can be determined from the change in the resistance.

From the results of XPS, reflectance, and TEM EDS measurements of the Co-doped ZnO SBs, we observed that Co exists in the form of Co^{2+}

and Co^{3+} in ZnO SBs. Moreover, Co^{3+} is known to act as a catalyst for organic molecular oxidation [27–29]. In air, Co^{2+} in the ZnO lattice reduces oxygen on the surface, and Co^{2+} is oxidized to form Co^{3+} , which donates electrons to the adsorption site of the reduced oxygen anion. Acetone can be oxidized at this site into water and carbon, and the activation energy for acetone oxidation is lower than that measured at the surface of undoped ZnO. Co^{3+} becomes Co^{2+} and forms oxygen vacancies around it, while acetone is oxidized. As a result, ZnO doped with Co exhibited a lower optimal working temperature and higher response compared to pure ZnO owing to the catalytic effect of Co ions.

4. Conclusions

In summary, we introduced sonochemically synthesized Co-doped ZnO SBs as the main material for constructing high-sensitivity acetone sensors with low working temperatures. ZnO SBs with a uniform size distribution were synthesized via a sonochemical process in an aqueous solution containing PEG and MEA.

ZnO SB is a promising material for high-sensitivity sensors because it has excellent gas permeability and high electrical contact resistance between ZnO SBs when stacked. In addition, to lower the working temperature of the sensor and increase the responsiveness of the acetone sensor, the ZnO SBs were doped with cobalt through a sonochemical process. The crystallinity, composition, and optical properties of the synthesized Co-doped ZnO SBs were analyzed. In particular, as the Co-doping concentration increased, the amount of substitutionally doped Co^{2+} in the ZnO lattice also increased. In addition, the fraction of Co^{3+} in the Co-doped ZnO SBs increased, while the fraction of O_v decreased.

Acetone sensors were fabricated using Co-doped ZnO SBs with various doping concentrations, whose performances were estimated. The undoped ZnO SB sensor exhibited an optimal operating temperature of 300 °C, whose response to 1 ppm acetone was 6. On the other hand, the 2 wt% Co-doped ZnO SB sensor showed the best performance among the Co-doped ZnO SB sensors, with an optimal working temperature of 250 °C and a response to 1 ppm of acetone of 7.9. To verify the practical applicability of the Co-doped ZnO SB sensor, the sensor was installed in a commercialized expiratory diagnostic device, through which the concentration of acetone contained in 1 ml of exhalation of a healthy adult was successfully measured to be 0.44 ppm. Compared to the undoped ZnO SB sensor, the Co-doped ZnO SB sensor exhibited a lower operating temperature and higher responsivity. This is because the Co^{3+} present in the Co-doped ZnO SB acted as a catalyst for acetone oxidation. We believe that the Co-doped ZnO SB has great potential as a key material for sensors that can detect sub-ppm levels of acetone gas contained in exhalation at low operating temperatures when used in an exhalation diagnostic device to monitor the effect of a ketogenic diet.

CRedit authorship contribution statement

Chang Hee Cho: Investigation, Data curation, Methodology, Writing – original draft. **Yong-Sahm Choe:** Conceptualization, Methodology, Data curation. **Soosang Chae:** Conceptualization, Supervision, Writing – review & editing. **Tae Il Lee:** Resources, Conceptualization, Supervision, Methodology, Writing – original draft, Writing – review & editing.

Declaration of Competing Interest

The authors declare that they have no known competing financial interests or personal relationships that could have appeared to influence the work reported in this paper.

Acknowledgements

This work was supported by the National Research Foundation of Korea (NRF) grant funded by the Korean Government (MSIP: Ministry of Science, ICT and Future Planning) (no. NRF-2020M2D9A3094171) and the Gachon University research fund of 2021(GCU- 202106570001).

Appendix A. Supplementary data

Supplementary data to this article can be found online at <https://doi.org/10.1016/j.ultsonch.2022.105956>.

References

- [1] Goldman-Cecil Medicine. 26th ed, Obesity. <https://www.clinicalkey.com>, 2020 (accessed 3 May 2021).
- [2] National Heart, Lung, and Blood Institute, Overweight and obesity. <https://www.nhlbi.nih.gov/health-topics/overweight-and-obesity>, 2021 (accessed 3 May 2021).
- [3] Conn's Current Therapy 2021, Obesity in adults. <https://www.clinicalkey.com>, 2021 (accessed 3 May 2021).
- [4] J.C.J.O. Anderson, Measuring breath acetone for monitoring fat loss, 23 (2015) 2327-2334.
- [5] K. Musa-Veloso, S.S. Likhodii, S.C.J.T.A.j.o.c.n. Cunnane, Breath acetone is a reliable indicator of ketosis in adults consuming ketogenic meals, 76 (2002) 65-70.
- [6] L.R. Saslow, S. Kim, J.J. Daubenmier, J.T. Moskowitz, S.D. Phinney, V. Goldman, E. J. Murphy, R.M. Cox, P. Moran, F.M.J.P.o. Hecht, A randomized pilot trial of a moderate carbohydrate diet compared to a very low carbohydrate diet in overweight or obese individuals with type 2 diabetes mellitus or prediabetes, 9 (2014) e91027.
- [7] The Insight Partners, Ketogenic Diet Market to Reach US\$ 15,640.6 Mn at CAGR of 5.5% in 2027. <https://www.theinsightpartners.com/reports/ketogenic-diet-market>, 2020 (accessed 4 November 2020).
- [8] E. Woelfenden, Monitoring VOCs in Air Using Sorbent Tubes Followed by Thermal Desorption-Capillary GC Analysis: summary of Data and Practical Guidelines, *J. Air Waste Manage. Assoc.* 47 (1) (1997) 20–36.
- [9] M. Leidinger, T. Sauerwald, W. Reimringer, G. Ventura, A.J.J.o.S. Schütze, S. Systems, Selective detection of hazardous VOCs for indoor air quality applications using a virtual gas sensor array, 3 (2014) 253-263.
- [10] A. Ulanowska, T. Kowalkowski, E. Trawińska, B.J.J.o.b.r. Buszewski, The application of statistical methods using VOCs to identify patients with lung cancer, 5 (2011) 046008.
- [11] A.D.J.S. Wilson, Application of electronic-nose technologies and VOC-biomarkers for the noninvasive early diagnosis of gastrointestinal diseases, 18 (2018) 2613.
- [12] A.W. Jones, L.J.F.s.i. Andersson, Comparison of ethanol concentrations in venous blood and end-expired breath during a controlled drinking study, 132 (2003) 18-25.
- [13] M.P.J.B.e.B.A.-G.S. Kalapos, On the mammalian acetone metabolism: from chemistry to clinical implications, 1621 (2003) 122-139.
- [14] V. Saasa, M. Beukes, Y. Lemmer, B.J.D. Mwakikunga, Blood ketone bodies and breath acetone analysis and their correlations in type 2 diabetes mellitus, 9 (2019) 224.
- [15] O.B. Crofford, R.E. Mallard, R. Winton, N. Rogers, J.C. Jackson, U.J.T.o.t.A.C. Keller, C. Association, Acetone in breath and blood, 88 (1977) 128.
- [16] V. Saasa, T. Malwela, M. Beukes, M. Mokgotho, C.-P. Liu, B.J.D. Mwakikunga, Sensing technologies for detection of acetone in human breath for diabetes diagnosis and monitoring, 8 (2018) 12.
- [17] Y. Kudo, S. Kino, Y.J.S. Matsuura, Vacuum Ultraviolet Absorption Spectroscopy Analysis of Breath Acetone Using a Hollow Optical Fiber Gas, Cell 21 (2021) 478.
- [18] A. Franco Jr, H.J.P.B.C.M. Pessoni, Enhanced dielectric constant of Co-doped ZnO nanoparticulate powders, 476 (2015) 12-18.
- [19] P. Kubelka, F.J.Z.T.P. Munk, An article on optics of paint layers, 12 (1931) 259-274.
- [20] P.J.J. Kubelka, New contributions to the optics of intensely light-scattering materials. Part 1, 38 (1948) 448-457.
- [21] X.-C. Liu, E.-W. Shi, Z.-Z. Chen, H.-W. Zhang, L.-X. Song, H. Wang, S.-D.J.J.o.c.g. Yao, Structural, optical and magnetic properties of Co-doped ZnO films, 296 (2006) 135-140.
- [22] J.Z. Sostaric, P. Mulvaney, F.J.J.o.t.C.S. Grieser, Faraday Transactions, Sonochemical dissolution of MnO₂ colloids, 91 (1995) 2843-2846.
- [23] M. Gutierrez, A.J.T.J.o.P.C. Henglein, Sonolytic decomposition of poly (vinylpyrrolidone), ethanol and tetranitromethane in aqueous solution, 92 (1988) 2978-2981.
- [24] M. Gutierrez, A. Henglein, J.K.J.J.o.P.C. Dohrmann, Hydrogen atom reactions in the sonolysis of aqueous solutions, 91 (1987) 6687-6690.
- [25] K.S. Suslick, *Ultrasound: its chemical, physical, and biological effects*, VCH Publishers, 1988.
- [26] R.V. Kumar, Y. Diamant, A.J.C.o.M. Gedanken, Sonochemical synthesis and characterization of nanometer-size transition metal oxides from metal acetates, 12 (2000) 2301-2305.
- [27] L. Liu, S. Li, J. Zhuang, L. Wang, J. Zhang, H. Li, Z. Liu, Y. Han, X. Jiang, P.J.S. Zhang, a.B. chemical, Improved selective acetone sensing properties of Co-doped ZnO nanofibers by electrospinning, 155 (2011) 782-788.
- [28] L. Hu, P. Zhang, Y. Sun, S. Bao, Q.J.C. Chen, ZnO/Co₃O₄ porous nanocomposites derived from MOFs: room-temperature ferromagnetism and high catalytic oxidation of CO, 14 (2013) 3953-3959.
- [29] X. Xie, Y. Li, Z.-Q. Liu, M. Haruta, W.J.N. Shen, Low-temperature oxidation of CO catalysed by Co₃O₄ nanorods, 458 (2009) 746-749.